Wave-Induced Sediment Transport and Sandbar Migration

Fernanda Hoefel[1] and Steve Elgar[2]

Onshore sediment transport and sandbar migration are important to the morphological evolution of beaches but are not well understood. Here, a model that accounts for fluid accelerations in waves predicts the onshore sandbar migration observed on an ocean beach. In both the observations and the model, the location of the maximum acceleration-induced transport moves shoreward with the sandbar, resulting in feedback between waves and morphology that drives the bar shoreward until conditions change. A model that combines the effects of transport by waves and mean currents simulated both onshore and offshore bar migration observed over a 45-day period.

Surf zone sandbars protect beaches from wave attack and are a primary expression of cross-shore sediment transport. During storms, intense wave breaking on the bar crest drives strong offshore-directed currents ("undertow") that carry sediment seaward, resulting in offshore sandbar migration (*1, 2*) (Fig. 1A). If the beach morphology is in equilibrium, the offshore migration is balanced by slower onshore transport between storms (*3, 4*). However, the causes of shoreward sediment transport and sandbar migration are not known, and thus models for beach evolution are not accurate (*1, 2, 5, 6*).

As waves enter shallow water, their shapes evolve from sinusoidal to peaky, with sharp wave crests separated by broad, flat wave troughs. It has been hypothesized that the larger onshore velocities under the peaked wave crests transport more sediment than the offshore velocities under the troughs (*7, 8*). However, models that account for the onshore-skewed velocities do not accurately predict onshore bar migration observed near the shoreline and in the surf zone (*1, 2, 5, 6*), although skewed velocities may be important outside the surf zone (*9*). As waves continue to shoal and break, they evolve from profiles with sharp peaks to asymmetrical, pitched-forward shapes with steep front faces. Water rapidly accelerates under the steep wave front, producing high onshore velocities, followed by smaller decelerations under the gently sloping rear of the wave (Fig. 1B) (*10, 11*). Large accelerations generate strong horizontal pressure gradients that act on the sediment (*12–14*). Although the precise mechanisms are not fully understood, it has been hypothesized that if accelerations increase the amount of sediment in motion (*10, 12, 15, 16*), there will be more shoreward than seaward transport under pitched-forward waves.

A surrogate for the effects of acceleration in pitched-forward waves is a dimensional form of acceleration skewness (*12*) (i.e., the difference in the magnitudes of accelerations under the front and rear wave faces), $a_{\mathrm{spike}} = \langle a^3 \rangle / \langle a^2 \rangle$, where a is the time series of acceleration and angle brackets denote averaging. Discrete-particle computer simulations of bedload transport driven by asymmetrical waves characteristic of surf zones indicate that sediment flux is proportional to a_{spike} once a threshold for sediment motion is exceeded (*12*). Unlike the monochromatic waves used in the numerical simulations, accelerations in random waves in a natural surf zone can be skewed either positively (onshore) or negatively (offshore). Thus, the expression for cross-shore (x) acceleration-driven bedload sediment transport $Q_{\mathrm{acc}}(x)$ suggested by the numerical simulations is extended to account for random waves by including a term that depends on the sign (i.e., the direction) of a_{spike}, yielding

$$Q_{\mathrm{acc}}(x) = \begin{cases} K_{\mathrm{a}}(a_{\mathrm{spike}} - \mathrm{sgn}[a_{\mathrm{spike}}]a_{\mathrm{crit}}) & \text{for } |a_{\mathrm{spike}}| \geq a_{\mathrm{crit}} \\ 0 & \text{for } |a_{\mathrm{spike}}| < a_{\mathrm{crit}} \end{cases} \quad (1)$$

where K_{a} is a constant, sgn[ ] is the sign of the argument, and a_{crit} is a threshold that must be exceeded for initiation of transport.

[1]Massachusetts Institute of Technology/Woods Hole Oceanographic Institution (WHOI) Joint Program in Oceanography, WHOI, Mail Stop 09, Woods Hole, MA 02543, USA. [2]WHOI, Mail Stop 11, Woods Hole, MA 02543, USA. E-mail: fhoefel@whoi.edu, elgar@whoi.edu

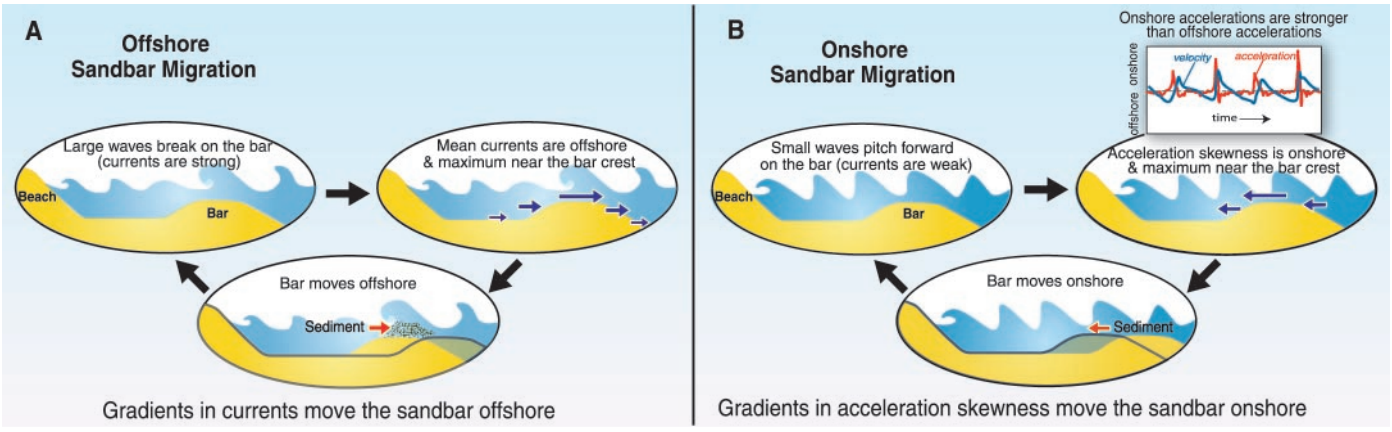

Fig. 1. Schematic of the feedbacks that drive sandbar migration. (**A**) Large waves in storms break on the sandbar, driving a strong offshore-directed current (undertow) that is maximum just onshore of the bar crest (*2*). The cross-shore changes (gradients) in the strength of the undertow result in erosion onshore, and deposition offshore of the sandbar crest, and thus offshore bar migration. The location of wave breaking and the maximum of the undertow move offshore with the sandbar, resulting in feedback between waves, currents, and morphological change that drives the bar offshore until conditions change. (**B**) Small waves do not break on the bar, but develop pitched-forward shapes. Water is rapidly accelerated toward the shore under the steep front face of the waves and decelerates slowly under the gently sloping rear faces. Thus, the time series of acceleration is skewed, with larger onshore than offshore values (rectangular panel). The cross-shore gradients in acceleration skewness (maximum on the bar crest) result in erosion offshore, and deposition onshore of the bar crest, and thus onshore bar migration. The location of the peak in acceleration skewness moves onshore with the sandbar, resulting in feedback between waves, currents, and morphological change that drives the bar onshore until conditions change.

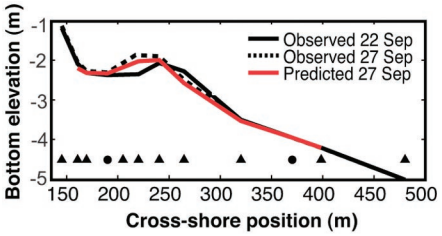

Fig. 2. Observed and predicted cross-shore bottom elevation profiles. Elevation of the seafloor relative to mean sea level observed on 22 September 1994, 1900 hours EST (black solid curve), observed on 27 September 1994, 1900 hours (black dashed curve), and predicted by the acceleration-based transport model (red curve) versus cross-shore position. The energetics transport model [using parameters in (*2*)] without acceleration predicts no change in the sea floor (*2*). Cross-shore locations of colocated pressure sensors, current meters, and altimeters are indicated by triangles, and locations of colocated pressure sensors and current meters by circles. Observed near-bottom velocities (sampled at 2 Hz) were low-pass filtered (cutoff frequency = 0.5 Hz) and differentiated in time to obtain near-bottom acceleration time series. Sediment transport fluxes for the model predictions were computed from 3-hour averages of observed near-bottom velocity and acceleration statistics, and integrated in time with a 3-hour time step (Eq. 2) to compute predicted bottom elevation changes. Mean sediment grain sizes ranged from 0.30 mm at the shoreline to 0.15 mm in water depth of 5 m (*2*).

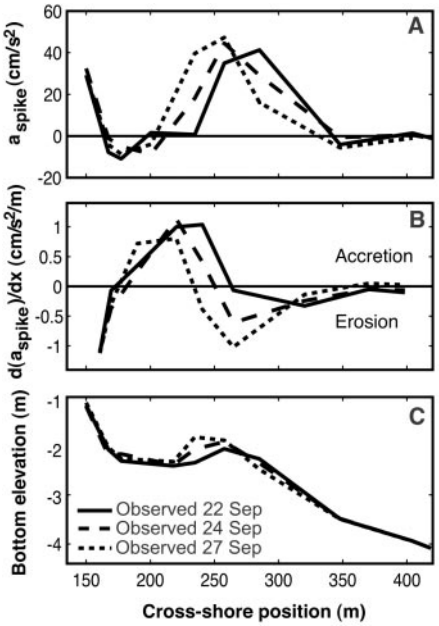

Fig. 3. Acceleration skewness and bottom elevation profiles during an onshore sandbar migration event. (**A**) Observed acceleration skewness (a_{spike}), (**B**) cross-shore gradient of acceleration skewness, and (**C**) sea-floor elevation relative to mean sea level versus cross-shore position. The solid curves are observations from 22 September 1994, 1900 to 2200 hours; dashed curves are 24 September 1994, 1300 to 1600 hours; and dotted curves are 27 September 1994, 1900 to 2200 hours.

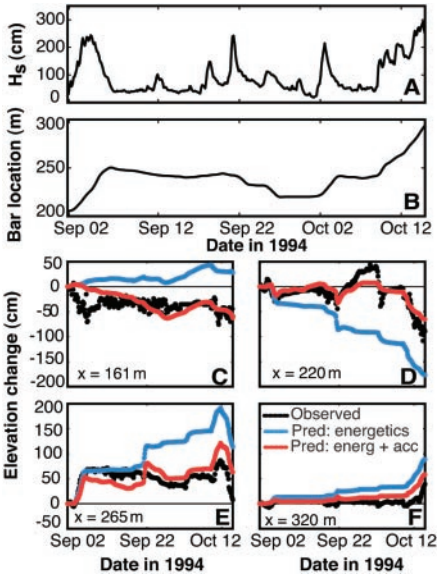

Fig. 4. Observed wave height, cross-shore sandbar crest position, and observed and predicted bottom elevation changes at four cross-shore locations between 1 September 1994, 1900 hours and 15 October 1994, 2200 hours. (**A**) Significant wave height (four times the standard deviation of 3-hour-long records of sea surface elevation fluctuations in the frequency bands between 0.01 and 0.3 Hz) observed in 5 m water depth and (**B**) cross-shore position of the sandbar crest versus time. The bar crest position was estimated from spatially dense surveys conducted with an amphibious vehicle approximately biweekly, combined with 3-hour estimates of sea-floor elevation from altimeter measurements (*2*) (Fig. 1). The shoreline fluctuated (owing to a 1-m tide range) about cross-shore location x = 125 m. Observed (black circles) and predicted (blue curve for energetics model, red curve for combined energetics and acceleration model) cumulative change in sea-floor elevation at cross-shore locations (**C**) x = 161 m, (**D**) x = 220 m, (**E**) x = 265 m, and (**F**) x = 320 m. Parameters in the energetics models are the same as those in (*2*).

By comparing model predictions with observations, the optimal values of $K_a = 1.40 \times 10^{-4}$ m s and of $a_{crit} = 0.20$ m s^{-2} were determined. These parameter values are within a factor of 5 of those suggested by the highly idealized discrete-particle numerical simulations (*12*) ($K_a = 0.26 \times 10^{-4}$ m s, $a_{crit} = 1.00$ m s^{-2}). Differences may be attributable to random waves, a distribution of sediment grain sizes and shapes, and breaking-induced turbulence in the ocean. If it is assumed that gradients in alongshore transport are negligible, mass conservation in the cross-shore direction yields

$$\frac{dh}{dt} = \frac{1}{\mu}\frac{dQ_{acc}(x)}{dx} \qquad (2)$$

where dh/dt is the change in bed elevation h with time t and $\mu = 0.7$ is a sediment packing factor. Extensions to Eq. 2 to account for alongshore changes are straightforward, but not necessary for the small alongshore gradients in transport inferred for the observations discussed here (*2*).

To test the hypothesis that the cross-shore distribution of near-bottom accelerations results in overall onshore sediment transport and sandbar migration when mean currents are weak, we compared morphological change predicted by the acceleration-based model (Eqs. 1 and 2) with observations made along a cross-shore transect extending about 400 m from the shoreline to 5 m water depth on the North Carolina coast (*2, 17*). The model was initialized (t = 0) with observed bathymetry and driven with accelerations observed with near-bottom–mounted current meters (Fig. 2). During a 5-day period with approximately 75-cm-high waves and cross-shore mean currents less than 30 cm s^{-1}, the observed onshore sandbar migration of about 30 m was predicted accurately (Fig. 2). A widely used energetics sediment transport model (*1, 2, 7, 8, 18*) that accounts for transport both by velocity skewness (but not acceleration) and by mean currents predicted no change in the cross-shore depth profile and thus failed to predict the observed sandbar migration (*2*).

During the onshore sandbar migration event, acceleration skewness (a_{spike}) increased from small values offshore to a maximum near the bar crest and then decreased toward the shoreline (Fig. 3, A and C), producing cross-shore gradients in transport that are consistent with erosion offshore and accretion onshore of the bar crest (Fig. 3, B and C). The peak in acceleration skewness moved shoreward with the bar crest (Fig. 3), resulting in feedback between wave evolution and bathymetry that promoted continued onshore sediment transport and bar movement until conditions changed (Fig. 1B). Feedback also occurs between wave-breaking–induced offshore-directed mean currents (maximum just onshore of the bar crest) and morphology that results in offshore bar migration during storms (*1, 2*) (Fig. 1A).

Inclusion of the effects of skewed accelerations (Eq. 1) in the energetics-based sediment transport model (*1, 2, 7, 8, 18*) resulted in improved predictive skill, both when mean cross-shore currents were weak (Fig. 2) and during storms when mean currents were strong (Fig. 4). During a 45-day observational period, the bar crest migrated offshore about 130 m during storms and onshore about 40 m when waves and mean flows were small (Fig. 4B), resulting in a net offshore migration of 90 m. Although

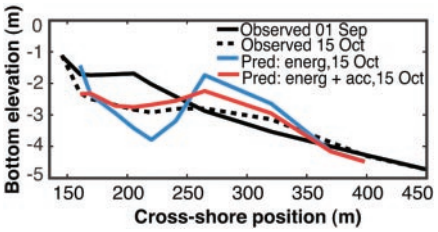

Fig. 5. Observed and predicted cross-shore bottom elevation profiles spanning a 45-day period. Sea-floor elevation relative to mean sea level observed 1 September 1994, 1900 hours (solid black curve), observed 15 October 1994, 2200 hours (dashed black), and predicted for 15 October 1994, 2200 hours by the energetics (blue) and energetics plus acceleration (red) models versus cross-shore position.

energetics models without acceleration-based transport predicted the offshore migration (*1, 2*), they had limited skill predicting the total change to the beach over 45 days because they failed to predict onshore migration between storms (*2*). The energetics model that was extended to include acceleration better predicted the change in the sea-floor both onshore and offshore of the bar crest (Fig. 4), and the overall evolution of the cross-shore depth profile (Fig. 5).

References and Notes

1. E. Thornton, R. Humiston, W. Birkemeier, *J. Geophys. Res.* **101**, 12097 (1996).
2. E. Gallagher, S. Elgar, R. Guza, *J. Geophys. Res.* **103**, 3203 (1998).
3. D. Aubrey, *J. Geophys. Res.* **84**, 6347 (1979).
4. L. Wright, A. Short, *Mar. Geol.* **56**, 93 (1984).
5. J. Roelvink, M. Stive, *J. Geophys. Res.* **94**, 4185 (1989).
6. L. Wright, J. Boon, S. Kim, J. List, *Mar. Geol.* **96**, 19 (1991).
7. A. Bowen, in *The Coastline of Canada*, S. McCann, Ed. (Geol. Surv. Canada Pap. 10-80, Ottawa, Canada, 1980), pp. 1–11.
8. J. Bailard, *J. Geophys. Res.* **86**, 10938 (1981).
9. J. Trowbridge, D. Young, *J. Geophys. Res.* **94**, 10971 (1989).
10. S. Elgar, E. Gallagher, R. Guza, *J. Geophys. Res.* **106**, 11623 (2001).
11. S. Elgar, R. Guza, M. Freilich, *J. Geophys. Res.* **93**, 9261 (1988).
12. T. G. Drake, J. Calantoni, *J. Geophys. Res.* **106**, 19859 (2001).
13. O. Madsen, in *Proc. 14th Int. Conf. Coastal Eng.*, Copenhagen, Denmark (American Society of Civil Engineers, Reston, VA, 1974), p. 776–794.
14. P. Nielsen, *Coastal Eng.* **45**, 53 (2002).
15. R. Hallermeier, *Cont. Shelf Res.* **1**, 159 (1982).
16. D. Hanes, D. Huntley, *Cont. Shelf Res.* **6**, 585 (1986).
17. E. Gallagher, S. Elgar, E. Thornton, *Nature* **394**, 165 (1998).
18. R. Bagnold, *U.S. Geol. Surv. Prof. Pap. 422-I* (1966).
19. Support was provided by the Army Research Office, the Office of Naval Research, NSF, and a fellowship from Conselho Nacional de Desenvolvimento Científico e Tecnológico (CNPq), Brazil. E. Gallagher, R. Guza, T. Herbers, and B. Raubenheimer made valuable comments and helped obtain the field observations. The staff of the Field Research Facility and the Center for Coastal Studies provided excellent logistical support during arduous field conditions.

12 December 2002; accepted 12 February 2003

Hexapod Origins: Monophyletic or Paraphyletic?

Francesco Nardi,[1]* Giacomo Spinsanti,[1] Jeffrey L. Boore,[2] Antonio Carapelli,[1] Romano Dallai,[1] Francesco Frati[1]

Recent morphological and molecular evidence has changed interpretations of arthropod phylogeny and evolution. Here we compare complete mitochondrial genomes to show that Collembola, a wingless group traditionally considered as basal to all insects, appears instead to constitute a separate evolutionary lineage that branched much earlier than the separation of many crustaceans and insects and independently adapted to life on land. Therefore, the taxon Hexapoda, as commonly defined to include all six-legged arthropods, is not monophyletic.

The phylum Arthropoda comprises the major groups Hexapoda (insects and presumed allies), Myriapoda (e.g., centipedes and millipedes), Chelicerata (e.g., spiders and horseshoe crabs), and Crustacea (e.g., crabs and lobsters). Many studies have attempted to reconstruct the evolutionary relationships among arthropods using various approaches such as paleontology (*1*), comparative morphology (*2*), comparative developmental biology (*3*, *4*), and molecular phylogenetics (*5*, *6*).

It has long been held that hexapods (*7*) constitute a monophyletic taxon (*8*, *9*) and that their closest relatives are to be found in myriapods (*10*). More recently, molecular and developmental studies have rejected this relationship (*3–5*, *11*, *12*) in favor of a closer affinity between Hexapoda and Crustacea (Pancrustacea or Tetraconata). In this context, special attention must be given to the apterygotes (springtails, silverfish, and their allies), the wingless hexapods thought to branch at the base of Hexapoda. The phylogenetic position of these groups is still unclear (*13–16*), casting doubt even on the monophyly of the Hexapoda (*17*).

A potentially powerful technique for resolving deep relationships is to compare whole mitochondrial genomes (*5*, *17*, *18*). Phylogenetic analysis of the only complete mitochondrial sequence available for an apterygotan species (*17*) suggested the possibility that Collembola might not be included within Hexapoda, contrasting with the classic view of a monophyletic taxon that includes all six-legged arthropods. Collembola have been clustered within crustaceans in other molecular and/or combined data sets (*15*, *16*), but the possible paraphyly of Hexapoda has not been given specific attention and the deserved consideration. We have now sequenced the complete mitochondrial genomes of two additional species (*19*) specifically chosen to address this problem: *Tricholepidion gertschi*, representing one of the most basal lineages of the Insecta (Zygentoma), and *Gomphiocephalus hodgsoni*, another collembolan, to test support for the two competing hypotheses of a monophyletic versus paraphyletic Hexapoda.

An initial phylogenetic analysis performed on the 35-taxon data set (*19*) produced the tree shown in Fig. 1. The tree has high support at most nodes, with support decreasing toward deeper relationships. This analysis strongly supports the Pancrustacea hypothesis, with the exception of the position of *Apis* and *Heterodoxus*. *T. gertschi* is basal to all the pterygotan insects, supporting the monophyly of the Insecta. The four crustacean sequences are divided into two well-defined groups (representing Malacostraca and Branchiopoda), but their reciprocal relationships and position relative to the Insecta are not resolved. The Crustacea + Insecta node is well supported, and it excludes the two collembolans, which cluster together as the basal lineage of the Pancrustacea. A second group unites the Chelicerata + Myriapoda [as in (*20*)] but also includes the insects *Apis* and *Heterodoxus*, presumably as an artefact.

Although this tree shows many interesting outcomes, it also contains some evidently untenable relationships, which nevertheless have strong statistical support. This indicates the presence of anomalies in the evolution of these sequences that introduce strong systematic errors in the analysis. The most likely factors that can cause these anomalies are unequal base composition [which can bias amino acid composition (*21*)] and uneven rates of evolution among different lineages. This problem might be especially acute, because some taxa share an extremely high AT bias—*Apis* (84.8%), *Rhipicephalus* (78.0%), and *Heterodoxus* (79.3%)—and different rates of evolution,

[1]Department of Evolutionary Biology, University of Siena, via Aldo Moro 2, 53100 Siena, Italy. [2]U.S. Department of Energy Joint Genome Institute and Lawrence Berkeley National Laboratory, 2800 Mitchell Drive, Walnut Creek, CA 94598, USA.

*To whom correspondence should be addressed. E-mail: nardifra@unisi.it